Examinating GPR based detection of defects in RC builds

Tahar Bachiri [1,*], *Mohammed* Hamdaoui[2], *Gamil* Alsharahi[2], *Mohammed* Bezzazi[1], and *Ahmed* Faize[2]

[1]Faculty of Sciences and Technology, Tangier 91001, Abdelmalek Essaadi University, Morocco
[2]Polydisiplinarly Faculty of Nador, Mohammed the First University, Morocco

Abstract. The Ground Penetrating Radar is a device which can be used for non-destructive inspection of civil engineering structures such as reinforced concrete buildings and bridges. Because of its ability to detect defects and provide reliable image of the substructure, it has attracted large interest from both practitioners and researchers in the field of health monitoring of vital structures. The objective of this work is to analyze detectability of defects in reinforced concrete structures by considering the presence of a defect which can attenuate GPR signals. Defects embedded in the structure can in fact cause significant changes in the intensity of the hyperbolic like reflection patterns generated by reinforcement bars. To assess this effect, a numerical simulation study of GPR data was conducted by using the GprMax software which is based on finite differences time domain method. The proposed approach has enabled to study the modification affecting the radargram due to the presence of a defect of finite size.

1 Introduction

Ground Penetrating Radar (GPR) is a non-destructive technique that has been successfully used in the evaluation of civil engineering structures, such as reinforced concrete structures and utilities buried under pavements or sidewalks [1-3]. For structures that need to be rehabilitated and which do not have detailed technical documents, the GPR is a precious tool for locating and determining the amount of rebars to be restored.

The GPR makes it possible to reveal in a non-destructive way the presence and the position of buried objects through the reflection of electromagnetic waves [4]. Previous studies have also demonstrated its capacity to detect armature corrosion [5]. Corrosion areas in rebars or degradation of concrete cause multiple distortions of the reflected signal from the concrete-bar interface. In GPR, all reflections that occur when electromagnetic waves are transmitted from one dielectric medium to another can be observed in the obtained radargram. For bridges, differences in the permittivities of asphalt, concrete, reinforcement bars, corrosion zones and cavities lead to the return of reflected signals [6].

Different procedures are employed to perform inspection by means of GPR. The A-scan trace provides initial information about the state of the substructure, but cannot be used to locate the defect. The B-scan and C-Scan which are formed by concatenating various A-scans that are taken during by moving the instrument along the X-axis (B-scan) or XY-plane (C-scan) enable to accede to more detailed information. They can be used to generate an image of the substructure.

For a point like target present in a homogeneous medium, the intensity of reflected signal during a B-scan generates a hyperbola curve in the radargram. This last is a representation of the acquired amplitude of reflected signal as function of the GPR antenna position. The shape, strength, and position of the hyperbolic profiles are influenced by the properties of the host medium and those of the target. In the case of reinforced concrete structure, the presence of moisture, air bubbles, corrosion areas, flaws causes reflection of the emitted GPR signal. These reflections are superimposed to those due to coming from the rebars. In addition to intrinsic signal attenuation in concrete, low intensity secondary reflections cause perturbations that affect visibility of GPR radargram.

The purpose of this paper is to investigate capacity of GPR in detecting defects present in reinforced concrete structures such as corrosion, moisture and voids. This consists of characterizing contrast variations of radargram due to these particular defects. The methodology used is base on field observation and numerical simulation.

2 Materials and methods

2.1 Theoretical background of GPR testing

GPR emits an electromagnetic pulse of shot duration which is centred on a given work frequency. These waves propagate at the speed

$$v=\frac{c}{\sqrt{\varepsilon_r \mu_r}} \quad (1)$$

where c is the wave speed in vacuum, ε_r and μ_r are respectively the relative permittivity and relative permeability of the medium.

* Corresponding author: tbachiri@uae.ac.ma

At the interface of two mediums having different dielectric constants, the coefficient of reflection of electromagnetic waves is given in [7]:

$$R=\frac{\sqrt{\varepsilon_1}-\sqrt{\varepsilon_2}}{\sqrt{\varepsilon_1}+\sqrt{\varepsilon_2}} \quad (2)$$

where ε_1 and ε_2 represent, respectively, the permittivity of the incident and reflective media. The contrast of permittivities is the main characteristic which is employed in GPR testing.

Electromagnetic waves are also attenuated during propagation. In low-loss materials, the attenuation coefficient α can be determined by the following approximation:

$$\alpha=\frac{\sigma+\varepsilon''(\omega)\omega}{2}\sqrt{\frac{\mu_0}{\varepsilon'(\omega)}} \quad (3)$$

where μ_0, σ and ε are respectively permeability in free space, conductivity of the medium and the complex dielectric permittivity, this last has the permittivities ε' and ε'' as real and imaginary parts and $\omega=2\pi f$ is the angular frequency in which f is the frequency.

2.2 A practical experiment

A real GPR testing was carried out on a reinforced concrete column having diameter of $30cm$. Fig.1 shows a photo with a description of B-scans that were performed.

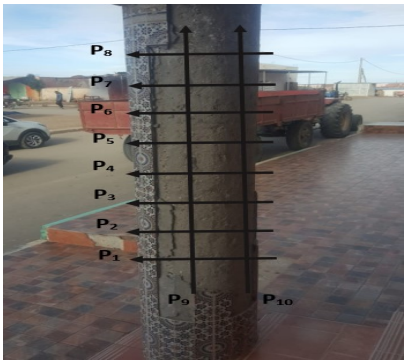

Fig. 1. Photo of a column with details of the inspection lines according to B-scan procedure.

The column was inspected by using the GPR system MALÅ CX from the company MALA Geosciences. The work frequency is $1.6GHz$ with the bandwidth laying from $0.8GHz$ to $2.4GHz$. The time window was fixed at $9ns$. Some of collected radargrams are presented in Fig. 2 and Fig. 3. These correspond to the two horizontal lines P6 and P7 and the vertical line P9.

In Figs. 2 and 3, the traces of reinforcing bars are visible as hyperbolic shape curves. The horizontal B-scans P6 and P7 show the existence of steel longitudinal rebars. Whereas the vertical B-scan shows the transverse rebars. One can use a radargram to determine the separation distance between rebars. It varies here between $15cm$ and $20cm$ for the scanning lines P6 and P7. One should note that the radargram give not a uniform trace for all rebars. This s because the concrete cover is not uniform or the dielectric constant varies. This may be explained either by the fact that cover concrete depth is not uniform or the permittivity of the medium is not homogeneous, may because of the presence of humidity in some zones. Other defects may be present in the column structure. To understand how some defects can modify the radargram content, a case of study is simulated in the following.

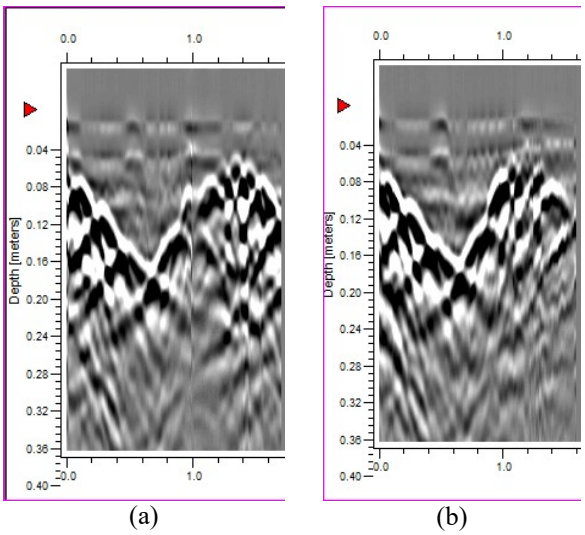

Fig. 2. B-scan radargram of the tested column: (a) horizontal line of scanning P6; (b) horizontal line of scanning P7.

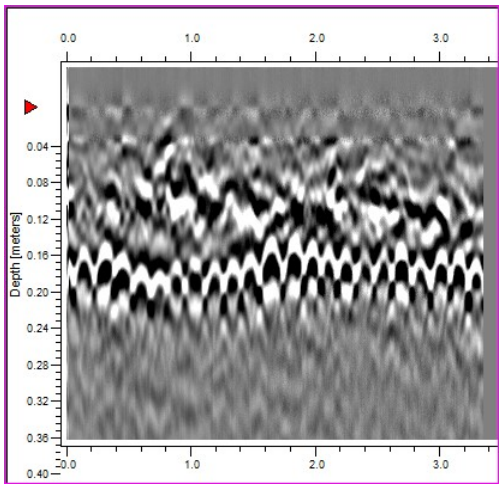

Fig. 3. B-scan radargram of the tested column associated to the vertical line of scanning P9.

2.3 Simulation of a case of study

Among the structural anomalies that can be found in reinforced concrete structures, one finds corrosion of rebars. Corrosion is an electrochemical process which results from the presence of moisture in concrete structures and is triggered by the presence of oxygen. It is categorized as a main cause of degradation observed in concrete structures. In health monitoring of a concrete structure, moisture is not considered a defect, but rather an indicator of the condition for structural evaluation. Other defects can also infect concrete structures such as

flaws and void cavities. This damage usually results in a reduction of strength and rigidity, which can be accompanied by fractures. In the literature, it has been reported that cracks greater than $2mm$ can produce reflections [8]. However, when the thickness of flaw decreased from $13mm$ to $1mm$, the trace of the reflection signal from this last flaw disappeared [9]. To detect a flaw in non reinforced concrete, the ratio between the wavelength of the signal in concrete and the thickness of the flaw must be greater than 50 [10]. Investigation should further be conducted in order to assess the capability of GPR to detect small defects and to characterize defect anomalies by post-processing reflection signal (A-scan) or GPR radargram (B-scan).

In the following, a case of study is considered in order to study traces of common defects present in RC structures. Simulation is performed by means of GprMax software which is based on the finite difference time domain (FTDT) method [10]. A rectangular part having dimensions $190cm \times 60m$, which is either concrete made or RC made with two layers of bars having diameter of $25mm$, is modelled under B-scan procedure. The antennas of transmission (Tx) and reception (Rx) have the fixed offset of $5cm$ and displaced along the length of the rectangular domain. A defect having the form of rectangular box of dimensions $40cm \times 5cm$ is assumed to be present in the concrete massif at the middle of the two rebars layers as illustrated in Fig. 4.

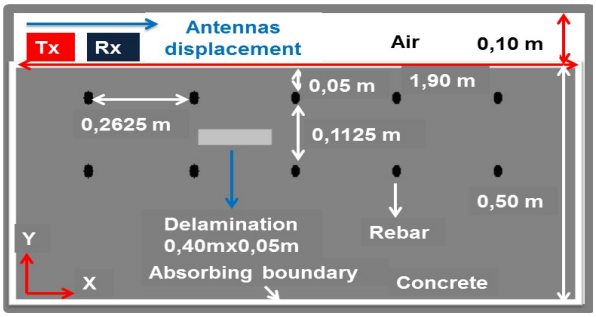

Fig. 4. Scheme of the simulated rectangular RC domain with indication of the positions of rebars and defect.

Table 1: Material parameters used in GPR simulation of the defected RC domain.

Medium	Permittivity ε_r	Permeability μ_r	Conductivity $\sigma(S/m)$
Concrete	$\varepsilon_{r1}=6\,;\varepsilon_{r2}=11$	1	$2\times10^{-11} f$
Air	1	1	0
Corrosion	25	$2-0.3j$	$5.56\times10^{-12} f$
Water	81	1	5×10^{-3}

The following command was used to generate this domain under GprMax: Box: 0.6 0.35 0.80 0.38. This defect area is assumed to be filled either by air, water of corroded steel materials. Their electromagnetic properties are given in Table 1. Rebar material is assumed to be a perfect conductor. The source pulse is Ricker centred on one of the following three frequencies: $f_1=1GHz$; $f_2=1.6GHz$ and $f_3=2.3GHz$. The domain was discretized by using a square mesh with space step equal to $2.5cm$ for both x and y directions. The total number of iterations is 1357.

3 Results and discussion

Considering the case without the box defect, Fig. 5 gives the obtained A-scan when using the $1.6GHz$ antenna and $\varepsilon_{r2}=11$. The curve shows a good resolution capacity in getting the location of the two layers of reinforcement by converting time into distance using the wave velocity.

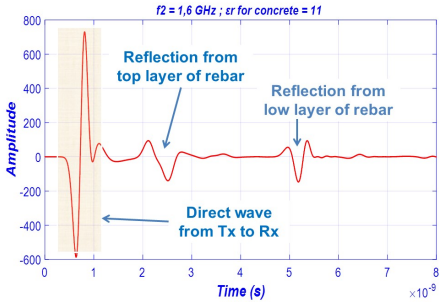

Fig. 5: Reflected signal from the two rebar layers.

In the following simulations both concrete permittivity values $\varepsilon_{r1}=6$ and $\varepsilon_{r2}=11$ as well as the three frequencies $f_1=1GHz$, $f_2=1.6GHz$ and $f_3=2.3GHz$ are used. The associated wavelengths of these frequencies for $\varepsilon_{r2}=11$ are: $\lambda_1=3.015mm$, $\lambda_2=1.88mm$ and $\lambda_3=1.31mm$. Note that the selected frequencies are used in most of commercially available antennas. A lower frequency leads to reduced ratio of wavelength by defect thickness, and so resolution. It was shown in [5] that, for a given thickness of the corrosion layer affecting corroded rebars, there are frequencies for which no distinction is visible between the corrosion layer and the corroded rebar layer.

Fig. 6a, 6b and 6c show that permittivity of concrete, type of defect material, as well as the work frequency, modify the sensed radargram in terms of intensities. However the trace of defect has the same pattern for all of them.

Figs. 7a, 7b and 7c show that intensity contrast of reflected signal varies a lot according the control parameters used. Contrast is higher with water filling the cavity than with air. Rebars can however continue to be well detected in the presence of the considered defect for the work frequencies and permittivities used.

Also, since rebars are perfect reflectors they prevent the propagation of electromagnetic waves from reaching the defect location. Trace of the defect appears only partially in the area where it is not hidden by the frames. Similar results were obtained in [11].

Detection of defects in concrete should take into account both attenuation associated to high frequencies, with short depth of penetration, and poor resolution with

low frequencies. When a defect is buried too deep and the frequency band chosen is too high, it can be undetectable. For RC structures the situation is more delicate as the defect trace could be shadowed by rebars.

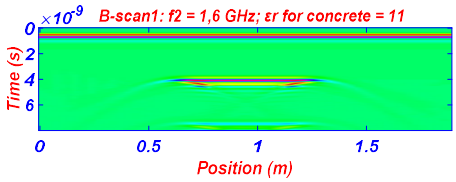

Fig. 6a: B-scan radargram associated to non reinforced concrete case with the box filled with air.

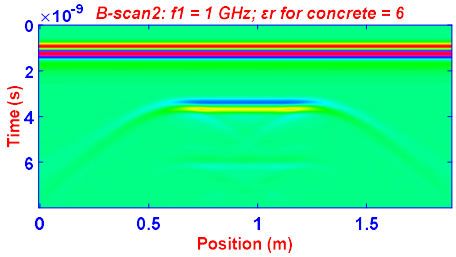

Fig. 6b: B-scan radargram associated to non reinforced concrete case with the box filled with corrosion material.

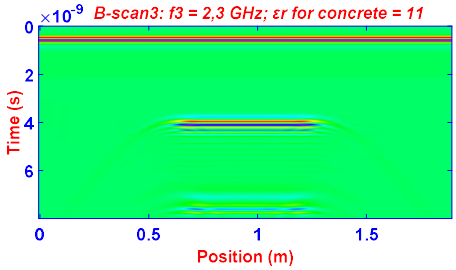

Fig. 6c: B-scan radargram associated to non reinforced concrete case with the box filled with water.

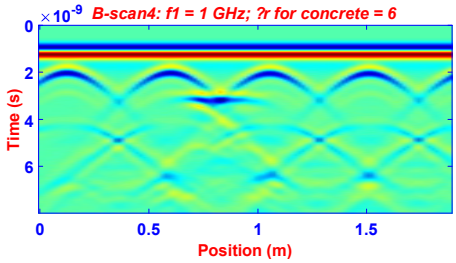

Fig. 7a: B-scan radargram associated to reinforced concrete case with the box filled with corrosion material.

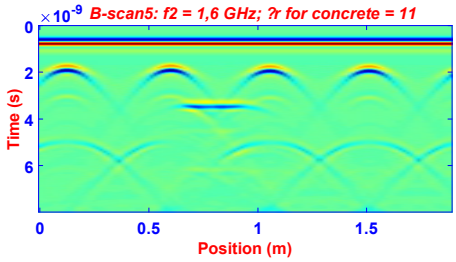

Fig. 7b: B-scan radargram associated to reinforced concrete case with the box filled with corrosion material.

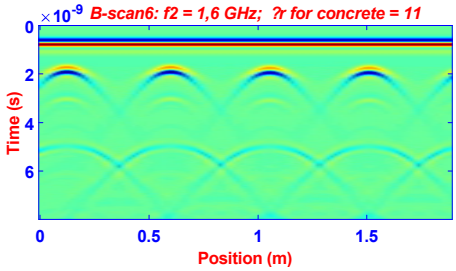

Fig. 7c: B-scan radargram associated to reinforced concrete case without defect.

4 Conclusions

In this paper, analysis of GPR detection of defect in RC structures was performed. The effect of key parameters on the reflected amplitudes was studied. It can be argued that GPR enables to display visible traces of some frequent defects present in RC structures. However, the GPR reflected signal depends hugely on the value of the dielectric constant, the size and depth of the defects and the work frequency used. The case of study has highlighted efficiency of GPR in detecting accurately defects of finite size present in a RC structure. It should be interesting to study in future work how reducing the size of the defect to a minimum can alter detectability.

References

1. J. Lachowicz, M. Rucka, Diagnostyka **16** (2015)
2. F. Tosti, C. Ferrante, Surveys in Geophy. **1**, 46 (2019)
3. T. Bachiri, G. Alsharahi, A. Khamlichi, M. Bezzazi, A. Faize, Int. J. of Emerg. Trends in Eng. Res. **8**, 5 (2020)
4. T. Bachiri, A. Khamlichi, M. Bezzazi, MATEC Web of Conf. **191**, 00004 (2018)
5. T. Bachiri, A. Khamlichi, M. Bezzazi, MATEC Web of Conf. **191**, 00009 (2018)
6. M. Scott, A. Rezaizadeh, M. Moore. *Phenomenology study of HERMES ground-penetrating radar technology for detection and identification of common bridge deck features* (Federal Highway Administration, McLean, 2001)
7. L. Jiao, Q. Ye, X. Cao, D. Huston, T. Xia, Measurement **160** (2020)
8. M. Heitzman, K. Maser, N.H. Tran, R. Brown, H. Bell, S. Holland, H. Ceylan, K. Belli, D. Hiltunen, Transp. Res. Board (2013)
9. A. Giannopoulos, Constr. and build. Mater. **19**, 10 (2005)
10. A. Tarussov, M. Vandry, A. de La Haza, Constr. and build. Mater. **38** (2013)
11. T. Bachiri, G. Alsharahi, A. Khamlichi, M. Bezzazi, A. Faize, *Ground Penetrating Radar Data Acquisition to Detect Imbalances and Underground Pipes* (Lecture Notes in Electrical Engineering, 745, Springer, Singapore, 2022)